Progress In Electromagnetics Research C, Vol. 118, 11–24, 2022

Defected Star-Shaped Microstrip Patch Antenna for Broadband Applications

Mahesh S. Pandey* **and Virendra S. Chaudhary**

Abstract—This research article proposes a Defected Star-Shaped Microstrip Antenna (DSSMSA) for wideband applications. A designed monopole antenna has a defected star-shaped tuning stub with a defected ground structure energised with a microstrip feed line. An appropriate tuning of resonating modes wideband frequency effect has been achieved by optimising the dimensions of the tuning stub and the dimensions of the defected ground and its notch. Surface current distribution plays a vital role in optimising the antenna geometry and developing mathematical resonating frequencies equations. The simulated and experimental results show that the DSSMSA radiates under the frequency band from 1.6638 GHz to 6.652 GHz with measured fractional bandwidth of 119.9692% for $|S_{11}| < -10$ dB. Optimised DSSMSA resonates at frequencies 2.05 GHz, 3.382 GHz, and 5.494 GHz. As the geometry of DSSMSA is symmetrical, the symmetric far-field pattern has been found in the far-field.

1. INTRODUCTION

Current wireless communications have different commercial wireless standards used for their organisation and allocated frequency band that radio equipment is used to transmit and receive the data [1]. They are nonstop to evolve from 1G to 5G, which could support higher capability digital systems with incorporated methods discussed in [2, 3].

In high data speed, wireless communications antennas must have a small size, good bandwidth, and omnidirectional characteristics [4]. These all above requirements could be easily reached by Monopole Antennas. That the arms of dipole or monopole have the nature of current distribution does not change the radiation patterns of the antenna; only it affects the input impedance [8].

Wideband frequency response for wireless data speeds and bandwidths to the internet for laptops, PDAs, and other wireless devices that operate close to one another and have evolved several times responding to the sustained user demands for higher bit-rates. GSM900, GSM1400, GSM1900, ISM, WLAN, Bluetooth, LTE, Wi-Fi, WiMAX come under the wideband applications [9–14].

Shukla et al. proposed a wideband antenna composed of an elliptical shape tuning stub and partial ground plane. The presented antenna was printed on an FR-4 substrate and achieved the impedance bandwidth of 116.32% over a frequency band from 1.23 GHz to 3.72 GHz [5].

Ellis presented a monopole antenna with a reduced ground plane by cutting a slot in a tuning stub and adding a strip in a slot for reducing the current distribution on the ground plane. This antenna was designed on an FR-4 substrate and provided the impedance bandwidth over the frequency range 3.6 GHz to 11 GHz [6].

Ghaderi and Mohajeri investigated a wide-slot antenna with a microstrip fed monopole antenna for UWB applications. The antenna was composed of an elliptic patch connected to a trapezoid, and a hexagonal slot was etched from a finite ground plane. The antenna substrate was FR-4 and achieved an impedance bandwidth of 145% over a frequency band from 2.9 to 18 GHz [7].

Received 2 November 2021, Accepted 12 January 2022, Scheduled 20 January 2022
* Corresponding author: Mahesh Shankar Pandey (mshankarpandey21@gmail.com).
The authors are with the Department of Electronics and Communication Engineering, RKDF University, Gandhinagar, Bhopal, India.

In this research investigation, a Defected Star-Shaped Microstrip Antenna (DSSMSA) has been reported, and its performance for improvement in impedance bandwidth and return loss ($-|S_{11}|$) is analysed. The reported antenna achieves the fractional bandwidth of 119.9692% for $|S_{11}| < -10$ dB over the frequency band from 1.6638 GHz to 6.652 GHz by a defected star-shaped tuning radiator with the defected ground structure (DGS) incorporated along with the notch in the centre. The reported antenna exhibits omnidirectional radiation properties. The reported DSSMSA finds itself a good candidate for broadband wireless services such as personal communication services (185–1.99 GHz), WiMAX (2.5 GHz, 3.5 GHz, and 5.5 GHz), and WLAN (2.4 GHz, 5.2 GHz, and 5.8 GHz). The performance characteristics such as antenna design, parametric analysis, input impedance, simulated surface current distribution, simulated and measured return losses, radiation pattern, and gain of reported antenna have been analysed.

2. ANTENNA GEOMETRY AND DESIGN

Figure 1 shows the structure of the designed antenna. The proposed DSSMSA is fabricated on an FR-4 substrate having thickness 1.6 mm, Loss Tangent ($\tan(\delta)0.02$, and dielectric constant (ε_r) = 4.3). The overall antenna geometry consists of a defected star-shaped radiator fed by a 50 Ω microstrip feed line. In the ground plane, a defected ground structure (DGS) is incorporated along with a notch in the centre in order to match proper impedance. By tuning the side cut and notch defection in the ground plane, the higher fractional bandwidth of 119.9692% is achieved over a frequency band from 1.6638 GHz to 6.652 GHz. The physical size of the proposed DSSMSA is 44 mm × 62 mm. The details of all dimensions are given in Table 1. The leaves of a defected star shape, notch, and both side cuts in ground have been incorporated in the antenna design to minimise the coupling between the edges of the patch and ground plane to improve the impedance matching ($|S_{11}| < -10$ dB). The proposed DSSMSA has been designed, simulated, and optimised on CST Microwave Studio.

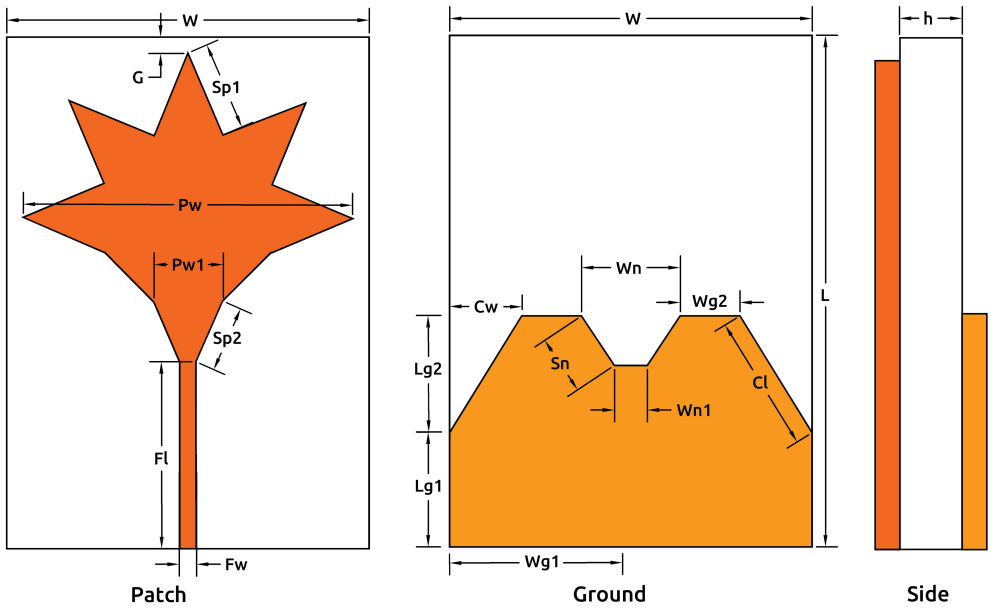

Figure 1. Configuration of proposed DSSMSA with 50 Ω microstrip feed line.

3. EVOLUTION OF ANTENNA

The evolution of the designed antenna is illustrated in Figure 2. The ground plane is modified in further succeeding steps to enhance the impedance bandwidth and accurate tuning of resonating modes. The return loss characteristics ($-|S_{11}|$) of all succeeding steps are depicted in Figure 3. Antenna 1 comprises

Table 1. Antenna dimensions.

Dimension	Value (mm)	Dimension	Value (mm)
W	44	L	62
F_l	22.65	L_{g1}	13.76
S_{p1}	10.8	L_{g2}	14.16
S_{p2}	8.06	C_w	8.5
P_w	40	W_{g1}	21
P_{w1}	8.3	W_{g2}	7.24
G	2	C_l	16.65
F_w	2	W_n	12
h	1.6	W_{n1}	4
S_n	7.81		

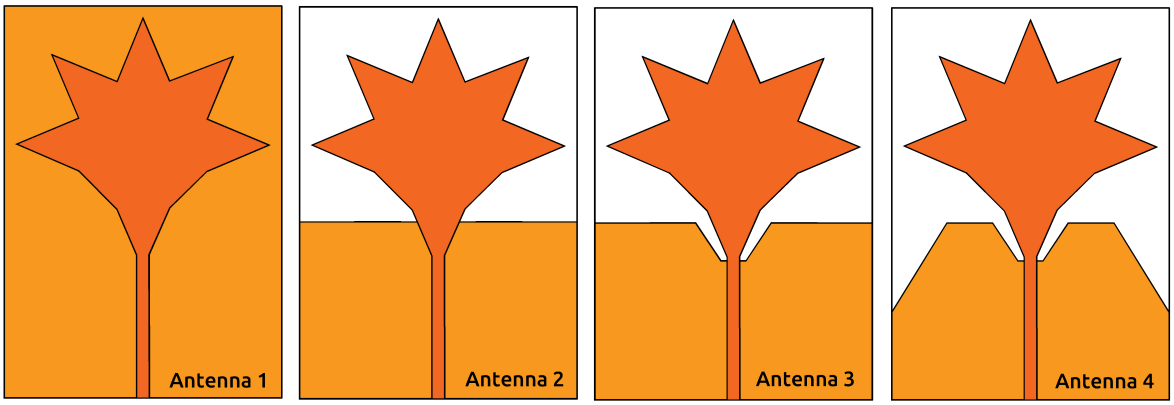

Figure 2. Evolution of antenna.

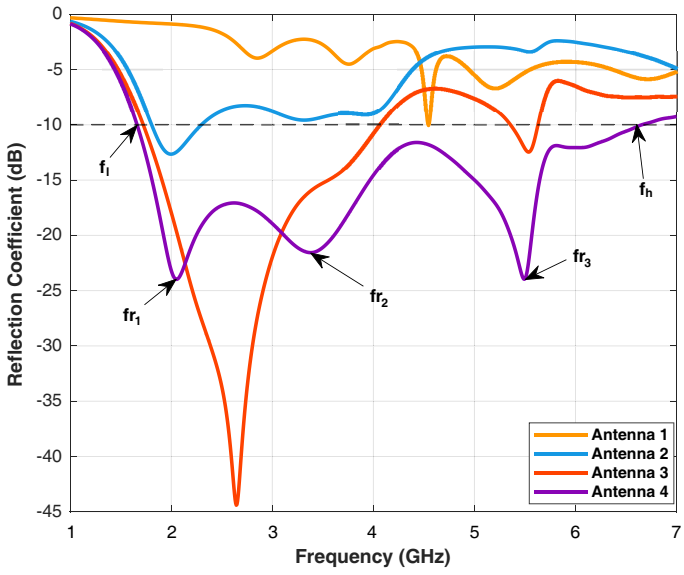

Figure 3. Return loss characteristics of Antenna 1 to 4.

a full ground structure, and at lower side two leaves (tuning element) have been removed from the star-shaped patch.

This antenna does not exhibit any band below −10 dB return loss which slightly touches the −10 dB line. The behaviour of first stage Antenna 1 is similar to a rectangular patch antenna which shows narrow bandwidth. In other stages, Antenna 2, the defected star-shaped tuning element with half defected ground structure (DGS), is integrated with this antenna which exhibits a single band of −12.24 dB reflection coefficient at 2 GHz.

Antenna 3 has the defected star-shaped tuning element with a half defected ground structure (DGS) integrated with this antenna which exhibits dual impedance bandwidth of 80.553% for $|S_{11}| < -10$ dB over the frequency band from 1.7257 to 4.0533 GHz and only 4.7% from 5.3726 to 5.6346 GHz.

In Antenna 4, the defected star-shaped tuning element has a half defected ground structure (DGS) and a notch in the centre of the ground plane. This antenna exhibits a single impedance bandwidth of 119.9692% for $|S_{11}| < -10$ dB over the frequency band from 1.6638 GHz to 6.652 GHz.

4. PARAMETRIC ANALYSIS

For the sake of optimising the antenna's performance for bandwidth performance and proper impedance matching, parametric analysis through parametric sweep has been performed on different structural parameters of the antenna. In this section, these additional parameters are varied within a specified range. The variation is also performed on one parameter at a time to get the exact impact on antenna performance.

4.1. Impact of Parameter Width (W_n) of Ground Notch

To see the impact on antenna's performance, one of the antenna parameters, notch width (W_n), has been varied. Notch width (W_n) is the top width of the notch made on the ground plane, opposite the joint of patch and feedline referring to Figure 4(a). The return loss characteristics have been recorded and illustrated in Figure 4(b) during variation. Notch width (W_n) is varied from 4 mm to 14 mm. During the variation of notch width, the bandwidth of antenna increases up to 12 mm. When Notch Width (W_n) is increased from 12 mm to 14 mm, the single band is divided into two bands, and effective bandwidth is decreased. So it can be concluded that 12 mm width is the optimum width for the notch to get the wider bandwidth.

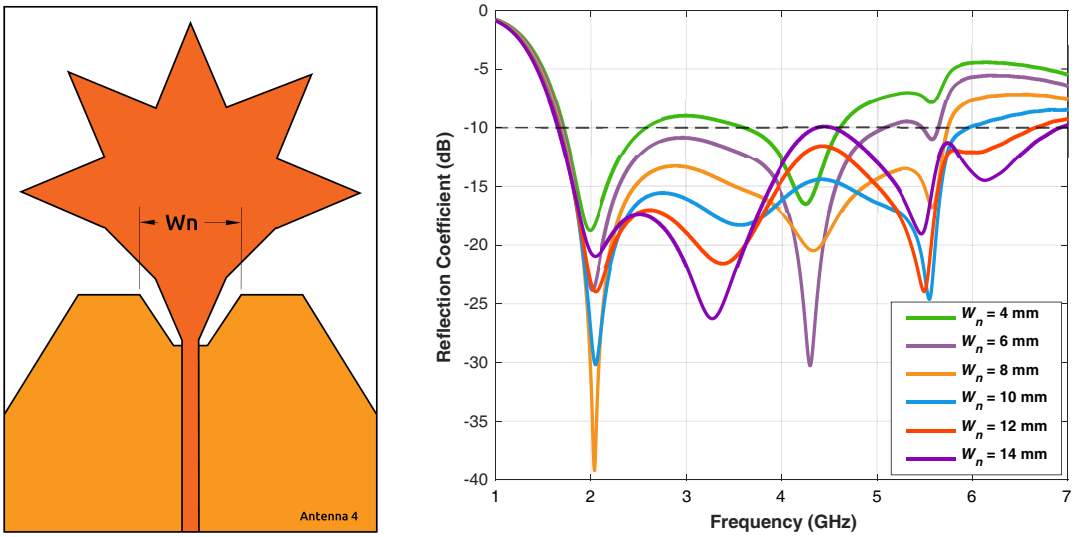

(a) (b)

Figure 4. Parametric analysis with notch width (W_n). (a) Antenna. (b) Impact on return loss characteristics.

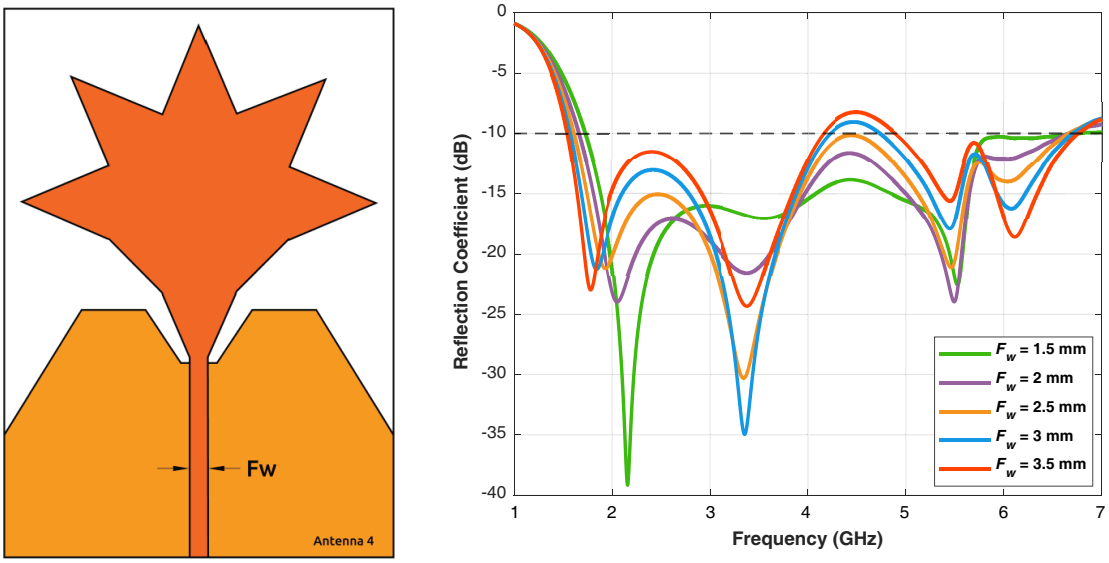

(a) (b)

Figure 5. Parametric analysis with feedline width (F_w). (a) Antenna. (b) Impact on return loss characteristics.

4.2. Impact of Parameter Feedline Width (F_w)

To see the impact on antenna's performance, another antenna parameter, feedline width (F_w), has been varied. F_w is the feedline width made on the patch plane referring to Figure 5(a). The return loss characteristics during the variation in F_w have been recorded and illustrated in Figure 5(b). F_w is varied from 1.5 mm to 3.5 mm. When F_w increases to 2 mm, the antenna's bandwidth reaches its maximum value. Further increment in F_w will create two bands, and effective bandwidth decreases. So it can be concluded that 2 mm feedline width is the optimum width for the feed to match the proper impedance of the antenna.

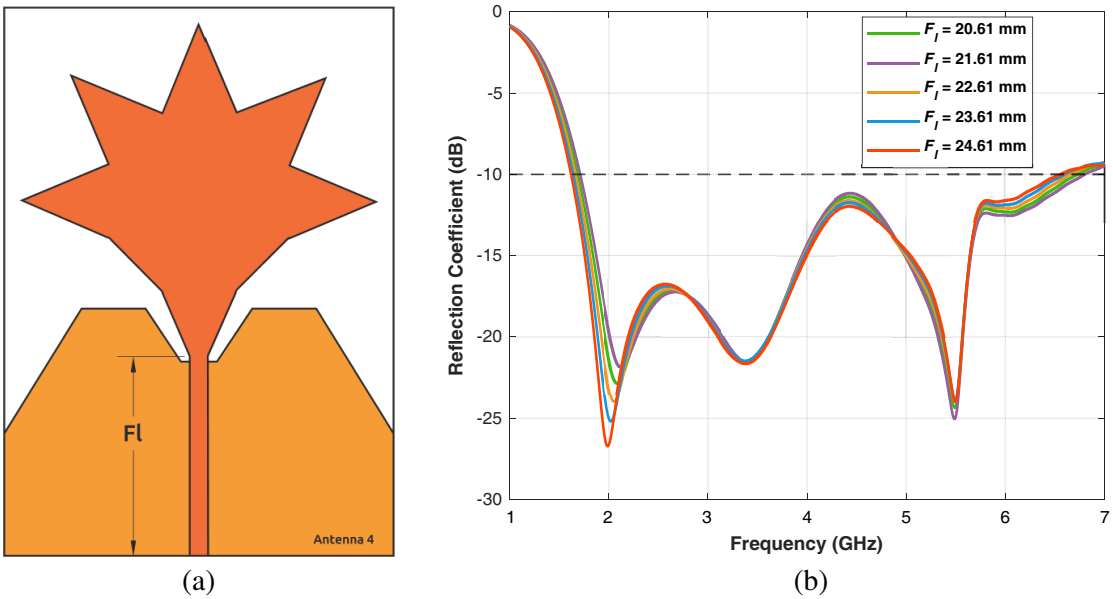

(a) (b)

Figure 6. Parametric analysis with feed length (F_l). (a) Antenna. (b) Impact on return loss characteristics.

4.3. Impact of Parameter Feedline Width (F_l)

To see the impact on antenna's performance, parameter feedline length (F_l) has been varied. F_l is the feedline length made on the patch plane refer to Figure 6(a). The return loss characteristics during variation have been recorded and illustrated in Figure 6(b). F_l is varied from 20.61 mm to 24.61 mm with a step size of 1 mm. The return loss characteristics show that the antenna's bandwidth decreases with a slight change when F_l increases. So it can be concluded that the variation in feedline length will not make any significant change in the antenna performance.

4.4. Impact of Parameter Feedline Width (P_w)

To see the impact on antenna's performance, parameter patch width (P_w) has been varied. P_w is the width of the patch from the left corner to the right corner on the patch plane referring to Figure 7(a). The return loss characteristics during variation have been recorded and illustrated in Figure 7(b). P_w is varied from 40 mm to 34 mm with a step size of 1 mm. The return loss characteristics show that when P_w decreases, the antenna's bandwidth increases with losses near 4.5 GHz, and it resonates on 3 GHz and 6.1 GHz. So it can be concluded that the variation in patch width will add 500 MHz bandwidth to existing bandwidth for 35 mm patch width in antenna performance.

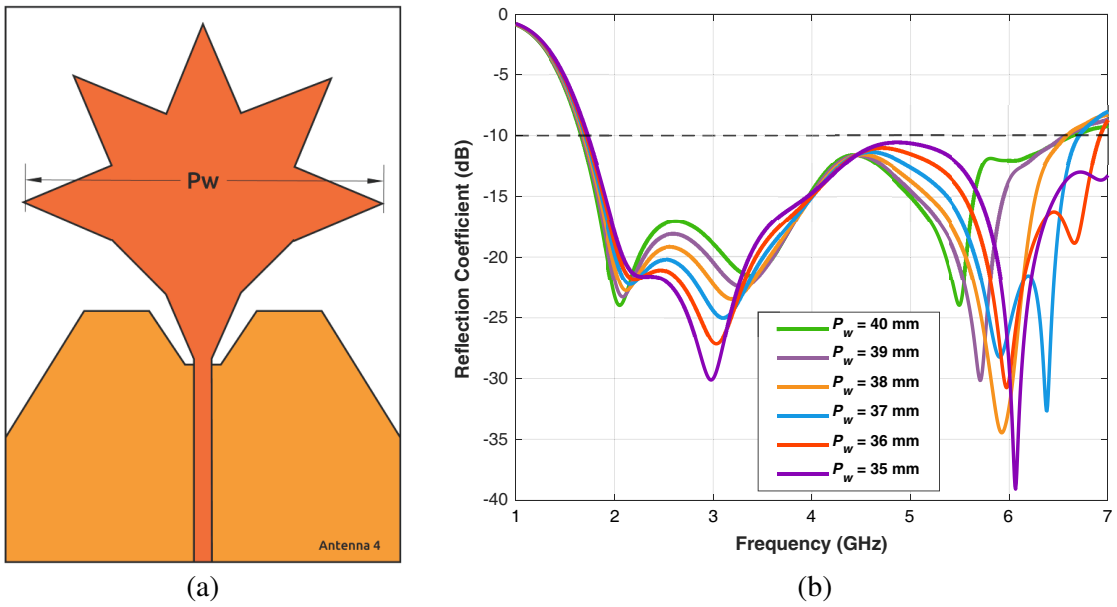

(a) (b)

Figure 7. Parametric analysis with patch size (P_w). (a) Antenna. (b) Impact on return loss characteristics.

4.5. Impact of Parameter Ground Top Corner Cut Length (C_l)

To see the impact on antenna's performance, parameter Ground Top Corner Cut Length C_l has been varied C_l is Parameter Ground Top Corner Cut Length referring to Figure 8(a). The return loss characteristics during variation have been recorded and illustrated in Figure 8(b). C_l is varied from 12.62 mm to 15.96 mm. The return loss characteristics show that when C_l increases, the return loss of antenna increases between 4 GHz and 6 GHz. So it can be concluded that the variation in cut length will add a slight increase in bandwidth to existing bandwidth for 15.96 mm patch width in antenna performance and a decrease in return loss around 5.5 GHz frequency.

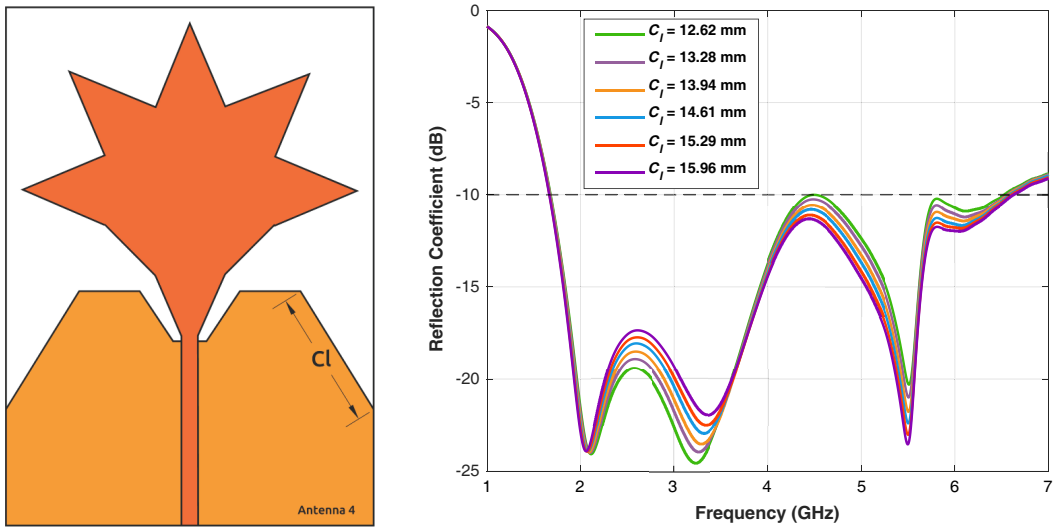

(a) (b)

Figure 8. Parametric analysis with ground top corner cut length (C_l). (a) Antenna. (b) Impact on return loss characteristics.

5. EXPERIMENTAL RESULTS AND DISCUSSION

The presented antennas' return loss characteristics show that the optimised Antenna 4 provides a good return loss curve at a lower cut-off frequency of 1.6638 GHz and a higher cut-off frequency of 6.652 GHz. The fabricated proposed antenna became a Broadband Antenna suitable candidate for wideband applications shown in Figure 9. It can be observed that the optimised antenna resonates at 2.05 GHz, 3.382 GHz, and 5.494 GHz in Figure 10.

$$\begin{aligned} \textit{Antenna Fractional Bandwidth} &= 2 \times \left(\frac{f_h - f_l}{f_h + f_l} \right) \times 100\% \\ &= 2 \times \left(\frac{6.652 - 1.6638}{6.652 + 1.6638} \right) \times 100\% \\ &= 2 \times \left(\frac{4.9882}{8.3158} \right) \times 100\% \\ \textit{Antenna Fractional Bandwidth} &= 119.9692\% \end{aligned} \tag{1}$$

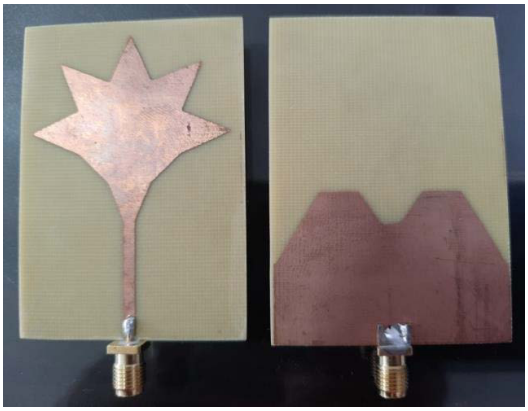

Figure 9. Fabricated antenna hardware front view (patch) and back view (ground).

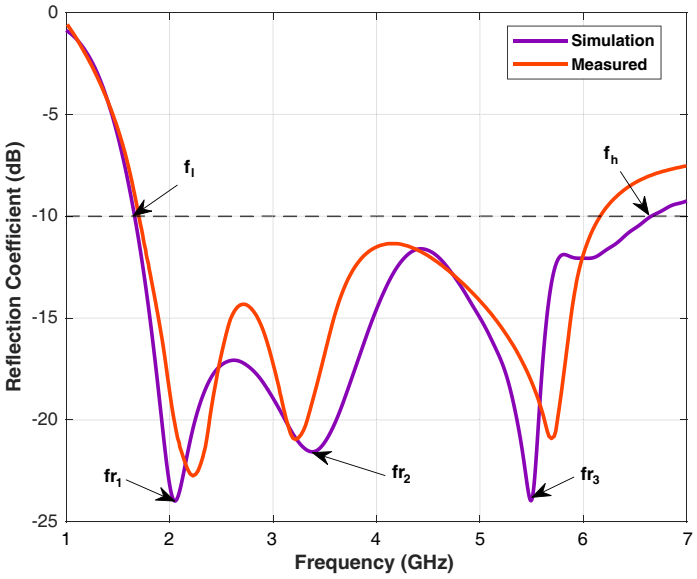

Figure 10. Reflection coefficient of simulation vs measured.

The designed antenna has provided the fractional bandwidth of 119.9692% from 1.6638 to 6.652 GHz frequency band calculated using Equation (1).

5.1. Reflection Coefficient Characteristics

Simulated and measured Reflection Coefficients $-|S_{11}|$ have been analysed. The measured results are obtained from Network Analyzer, and the frequency band from 1.6638 GHz to 6.652 GHz with measured fractional bandwidth of 119.9692% for $|S_{11}| < -10$ dB is found. They resonate (measured) at frequencies 2.35 GHz, 3.1 GHz, and 5.7 GHz. Optimised DSSMSA resonates (simulated) at frequencies 2.05 GHz, 3.382 GHz, and 5.494 GHz. A small error has been found between simulated and measured results. The dielectric constants of connector and conductor are different because the materials are different. The power transferring from one material to another material creates mismatches and losses. That is the

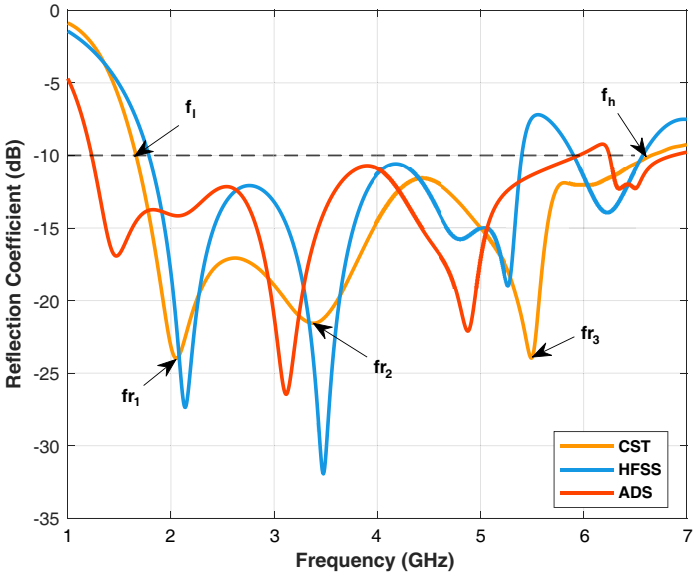

Figure 11. Reflection coefficient of CST vs ADS vs HFSS.

reason of error.

In Figure 11, proposed antenna's results have been simulated, and obtained results are verified in CST, ADS, and HFSS, with slight difference between them. The ADS equivalent circuit is shown in Figure 12.

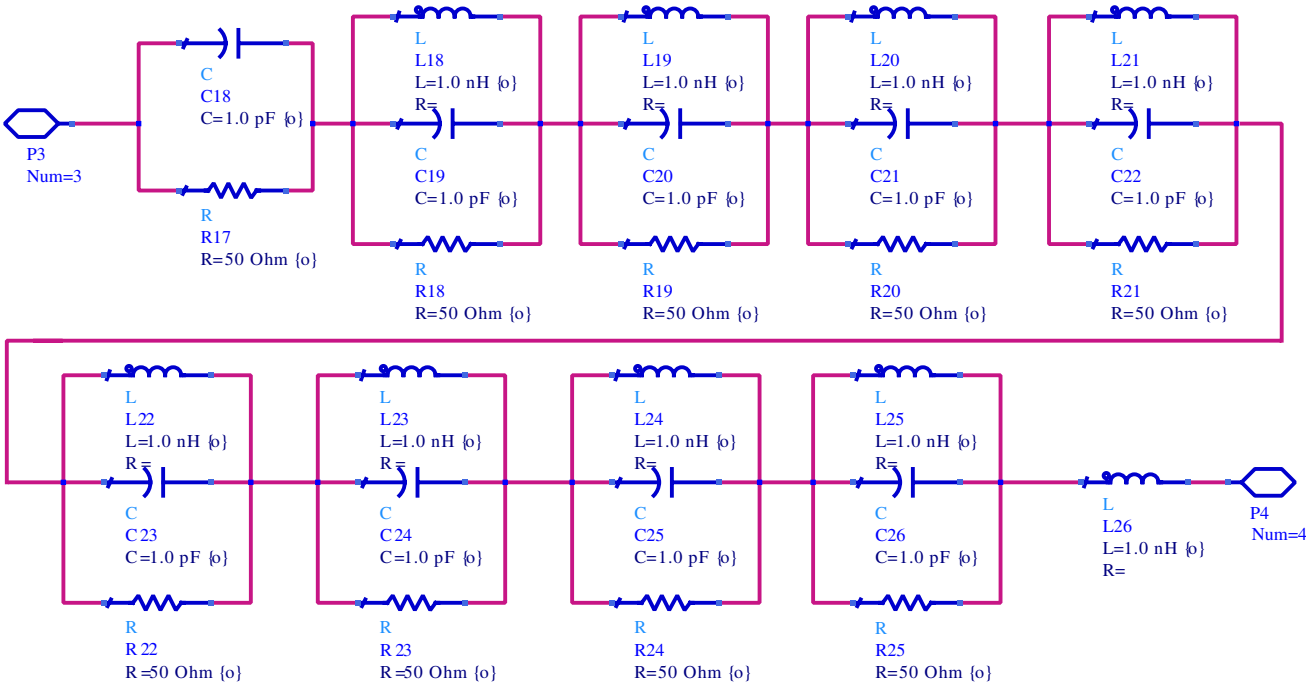

Figure 12. ADS equivalent circuit of proposed antenna.

5.2. Surface Current Distribution

To analyse the current distribution on antenna surface, in CST, the resonant frequencies 2.05 GHz, 3.382 GHz, and 5.494 GHz were used for surface current distribution analysis, respectively. This analysis helps identify which part of the antenna is responsible for generating a specific frequency range. The simulation has been performed in CST-MWS and is shown in Figure 13.

5.2.1. First Resonance

At the first resonance frequency of 2.05 GHz, the current vectors originate from the feedline's bottom and travel towards the patch triangle's top. The maximum intensities of current vectors are found near the joint of the patch triangle and feedline. The 2.05 GHz frequency signal is a result of the side edges of the patch. This path starts from the lower end of the feedline to the top side of the patch triangle. The current path can be determined by Equation (2).

$$\begin{aligned} P_1 &= F_l + S_{p2} + P_{w1} + 3 \times S_{p1} \\ &= 22.65 + 8.06 + 8.3 + 3 \times 10.8 \\ &= 71.41 \text{ mm} \end{aligned} \tag{2}$$

The computed length of the current path P_1 is 71.41 mm, and the calculated value of f_{r1} is 2.09 GHz (using Equation (3)). The difference between actual and calculated frequencies is 1.95%. This can be caused by environmental factors and other losses.

$$f_{r1} = \frac{c}{P_1\sqrt{\varepsilon_r}} \tag{3}$$

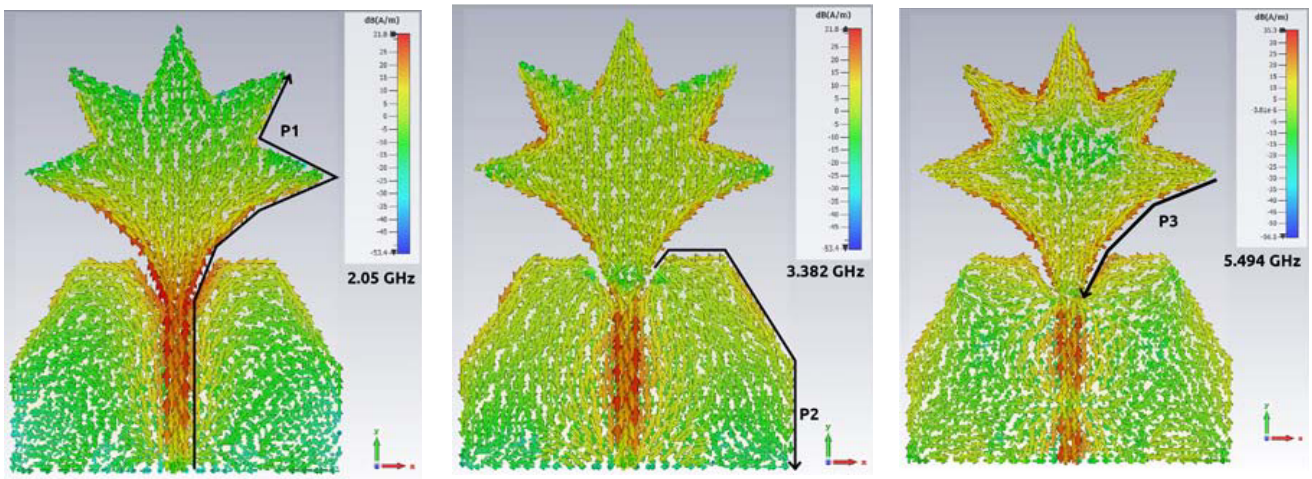

Figure 13. Surface current distribution on resonant frequencies. (a) 2.05 GHz, (b) 3.382 GHz, and (c) 5.494 GHz.

5.2.2. Second Resonance

At the second resonance frequency of 3.382 GHz, the current vectors in the ground plane sink at the bottom corners originating from notch travelling through the edges. The maximum intensities of current vectors are found around C_l (side cuts on ground plane). So, from the current analysis, it is clear that 3.382 GHz frequency signals are produced by the side edges of the ground plane from the notch to bottom corner of the ground. The following path can be determined by Equation (4).

$$\begin{aligned} P_2 &= S_n + W_{g2} + C_l + L_{g1} \\ &= 7.81 + 7.24 + 16.65 + 13.76 \\ &= 45.46\,\text{mm} \end{aligned} \tag{4}$$

The computed length of the current path P_2 is 45.46 mm, and the respective calculated value of resonance frequency f_{r2} is 3.29 GHz (using Equation (5)). The difference between actual and calculated frequencies is 2.72%. Environmental factors and other losses can cause this.

$$f_{r2} = \frac{c}{P_2\sqrt{\varepsilon_r}} \tag{5}$$

5.2.3. Third Resonance

At the third resonance frequency 5.494 GHz, the current vectors sink from the lower middle point of the feedline and side corners of the patch triangle towards the joint of the patch triangle and feedline. The maximum intensities of current vectors are found around the patch triangles and side edges of the feedline. So, from the current analysis, it is clear that 5.494 GHz frequency signals are produced by the side edges of the patch only. Equation (6) will be used to determine the path.

$$\begin{aligned} P_3 &= S_{p2} + P_{w1} + S_{p1} \\ &= 8.06 + 8.3 + 10.8 \\ &= 27.16\,\text{mm} \end{aligned} \tag{6}$$

The computed length of the current path, P_3, is 27.16 mm, and the calculated value of f_{r3} is 5.52 GHz (using Equation (7)). The difference between actual and calculated frequencies is 0.47%. Environmental factors and other losses may be the reason for this.

$$f_{r3} = \frac{c}{P_3\sqrt{\varepsilon_r}} \tag{7}$$

The summary of theoretical and practical resonance frequencies and the current path computed from antenna dimensions are given in Table 2.

Table 2. Theoretical and actual current path calculations for resonance frequencies.

Resonance Frequency	Actual Values (GHz)	Computed Resonance Frequency (GHz)	Error (%)	Current Path	Actual Path Length (mm)
f_{r1}	2.05	2.09	1.95	P_1	71.41
f_{r2}	3.382	3.29	2.72	P_2	45.46
f_{r3}	5.494	5.52	0.47	P_3	27.16

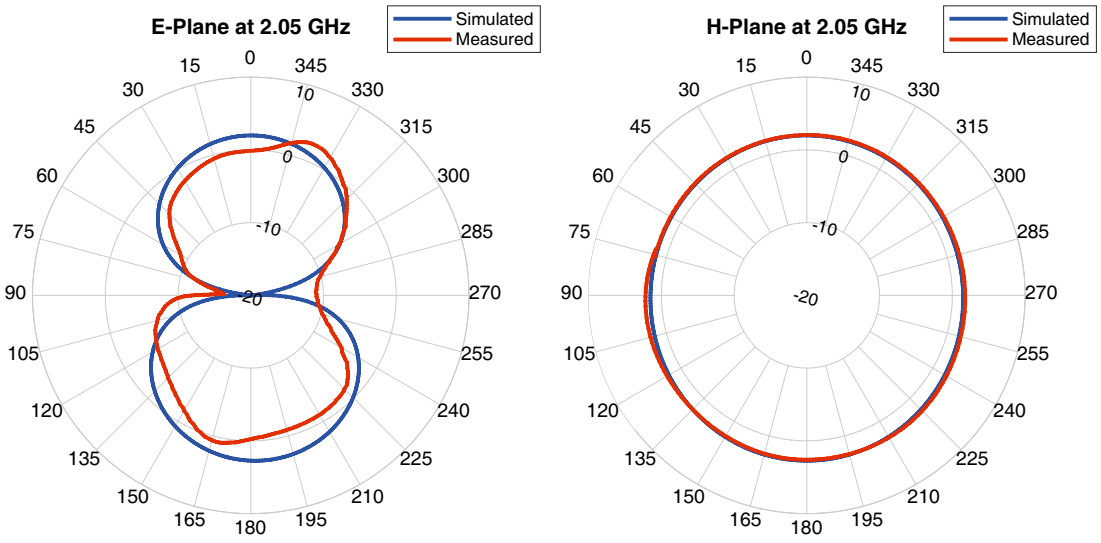

(a)

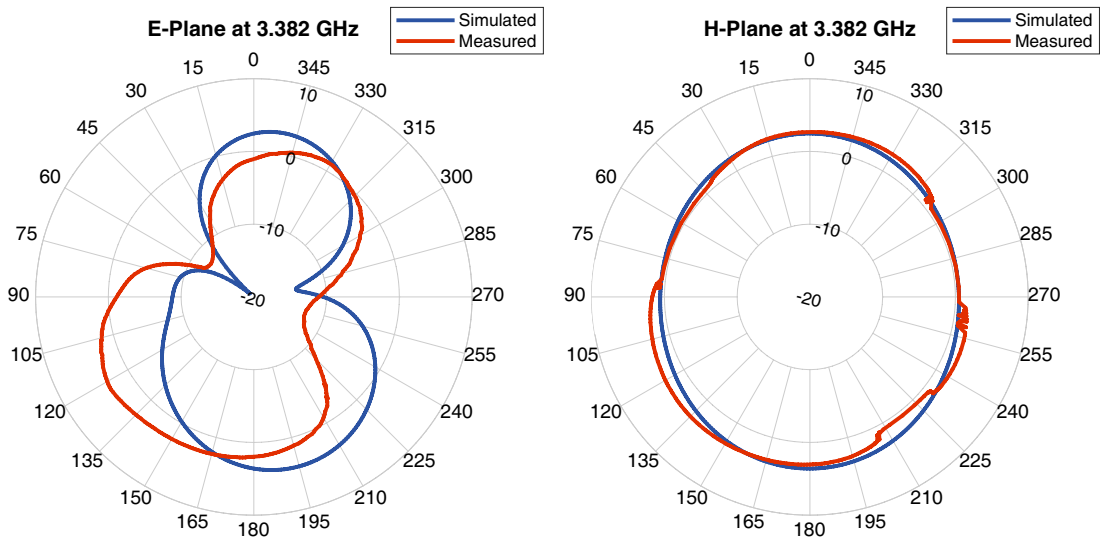

(b)

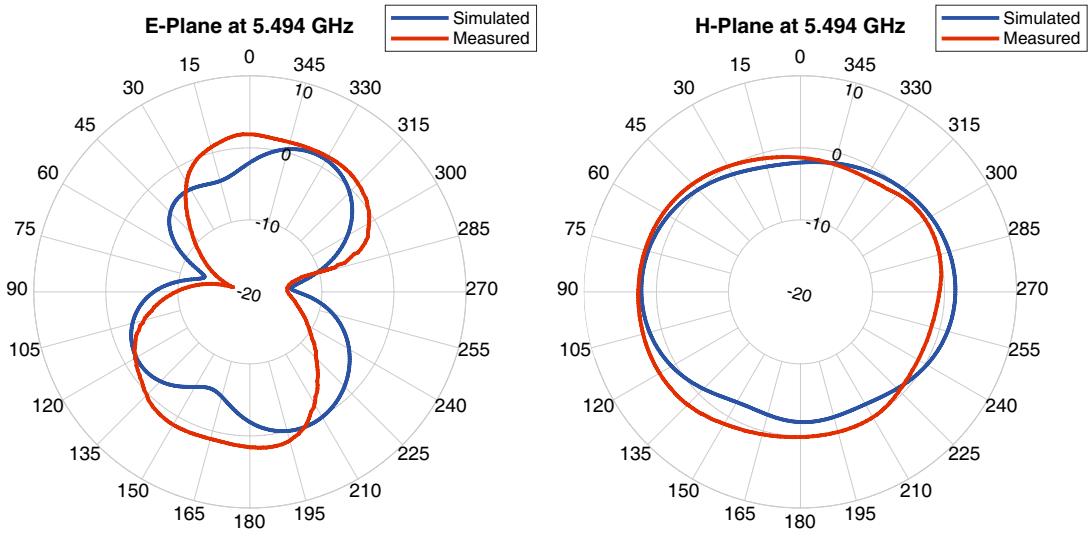

(c)

Figure 14. 2D far-field radiation patterns of E and H planes at (a) 2.05 GHz, (b) 3.386 GHz, and (c) 5.494 GHz.

5.3. Far-Field Pattern

The analysis between simulated and measured far-field radiation patterns results has been performed, and it is found that they slightly vary due to surrounding environment of measuring instruments or fabrication error (refer Figure 14). At the resonating frequencies 2.05 and 3.382 GHz, a far-field pattern has been found omnidirectional in E-plane and H-plane. The efficiency of the presented antenna is declined due to dielectric loss (see Figure 17). The realised gain of the proposed antenna varies from 2.4 to 3.5 dBi (see Figure 18).

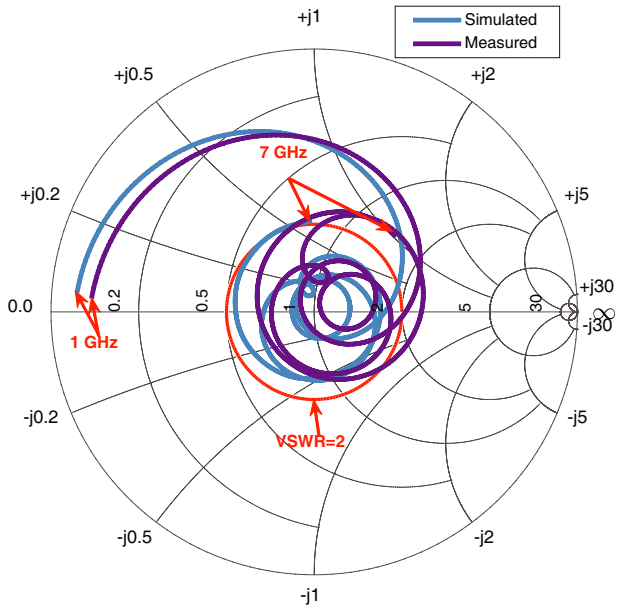

Figure 15. Impedance curve.

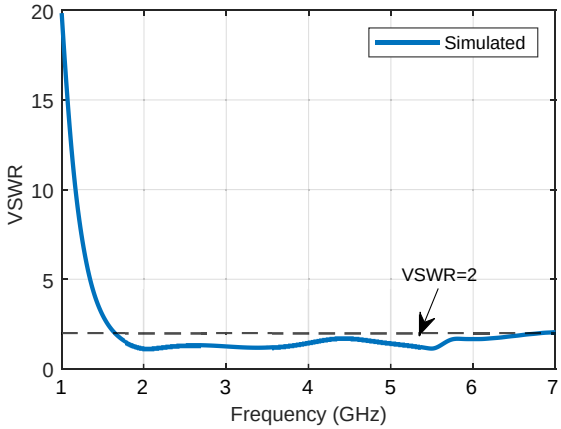

Figure 16. VSWR (simulated) curve of the proposed antenna.

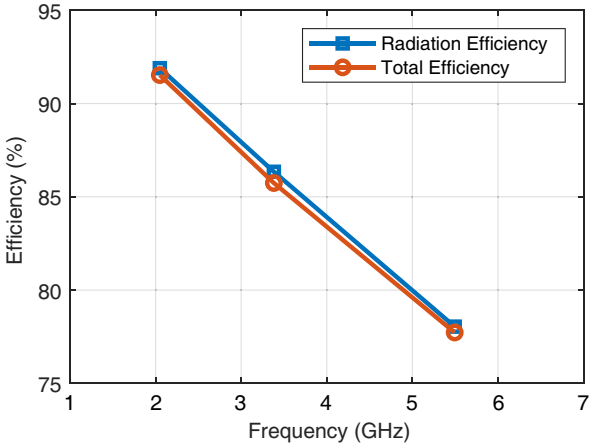

Figure 17. Simulated radiation efficiency and total efficiency of the proposed antenna.

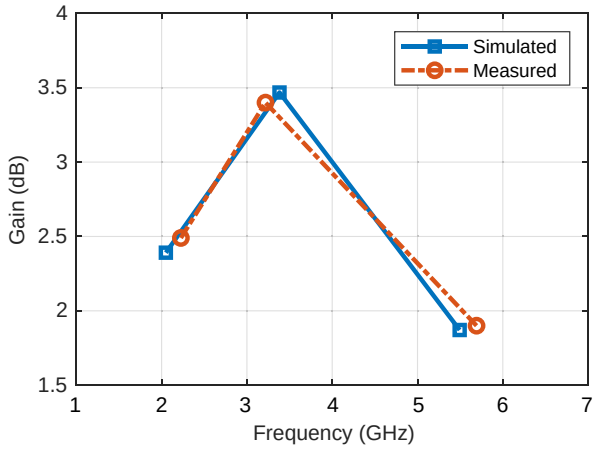

Figure 18. Gain of antenna.

5.4. Input Impedance

The input impedance of the designed antenna is presented in Figure 15. It is observed that multiple loops are found inside the VSWR circle, indicating the mutual coupling and overlapping between resonating modes, which are essential for wide impedance bandwidth (refer to Figure 16).

In Table 3, the proposed antenna has been compared with other antennas and found a good candidate in terms of high bandwidth and compact structure in size of the antenna.

Table 3. Performance comparison of the proposed antenna with other surveyed antennas.

References	f_l (GHz)	f_h (GHz)	BW (%)	Gain (dB)	Size (W × H) mm^2
[5]	1.23	4.65	116.32		$0.53\lambda_g \times 0.75\lambda_g$
[11]	1.347	1.533	12.91	4.3	$0.71\lambda_g \times 0.71\lambda_g$
[12]	4.53	7.47	49	4.1	$1.3\lambda_g \times 0.99\lambda_g$
[13]	3.4	5.6	49.4	4.8	$1.55\lambda_g \times 1.55\lambda_g$
[14]	1.639	1.907	15.11	5	$1.08\lambda_g \times 1.08\lambda_g$
[15]	1.80	6.09	108.74	5	$1.05\lambda_g \times 1.25\lambda_g$
Proposed	1.6638	6.652	119.96%	3.5	$0.52\lambda_g \times 0.74\lambda_g$

6. CONCLUSION

In this research work, a Defected Star-Shaped Microstrip Antenna (DSSMSA) has been designed and studied for improvement in impedance bandwidth and return loss ($-|S_{11}|$) characteristics. Optimised DSSMSA achieves the fractional bandwidth of 119.9692% for $|S_{11}| < -10$ dB over the frequency band from 1.6638 GHz to 6.652 GHz. Radiation patterns and current distributions at resonating frequencies 2.05 GHz, 3.382 GHz, and 5.494 GHz were investigated and found omnidirectional at resonating frequencies with 3.45 dBi gain at 3.4 GHz and -24 dB maximum return loss at 5.5 GHz. The simulated and measured results show that the presented antenna is an attractive candidate for wideband applications such as WiMAX and WLAN.

REFERENCES

1. Evans, J. A. and M. J. Ammann, "Planar trapezoidal and pentagonal monopoles with impedance bandwidths in excess of 10 : 1," *Proc. IEEE Antennas Propag. Symp.*, Vol. 3, 1558–1561, 1999.
2. Ammann, M. J. and Z. N. Chen, "A wideband shorted planar monopole with bevel," *IEEE Transactions on Antennas and Propagation*, Vol. 51, 901–903, 2004.
3. Liang, X. L., S. S. Zhong, and W. Wang, "UWB printed circular monopole antenna," *Microw. Opt. Tech. Lett.*, Vol. 48, 1532–1534, 2006.
4. Zhang, Y., Z. N. Chen, and M. Y. W. Chia, "Effects of finite ground plane and dielectric substrate on planar dipoles for UWB applications," *Proc. IEEE Int. Symp. Antennas Propagation*, 2512–2515, 2004.
5. Shukla, B. K., N. kashyap, and R. K. Baghel, "A novel design of Scarecrow-shaped patch antenna for broadband applications," *International Journal of Microwave and Wireless Technologies*, page 1 of 9, Cambridge University Press and the European Microwave Association, 2017.
6. Ellis, M. S., Z. Zhao, J. Wu, Z. Nie, and Q. H. Liu, "Small planar monopole ultra wideband antenna with reduced ground plane effect," *IET Microw. Antennas Propag.*, Vol. 9, 1028–1034, 2015.
7. Ghaderi, M. R. and F. Mohajeri, "A compact hexagonal wide slot antenna with microstrip fed monopole for UWB application," *IEEE Antennas Wireless Propag. Lett.*, Vol. 10, 682–685, 2011.
8. Wong, K. L., C. H. Wu, and S. W. Su, "Ultrawideband square planar metal-plate monopole antenna with a trident-shaped feeding strip," *IEEE Transactions on Antennas and Propagation*, Vol. 53, 1262–1269, 2005.
9. Paulsen, L., J. B. West, W. T. Perger, and J. Kraus, "Recent investigation of the volcano smoke antenna," *Proc. IEEE Antennas Propag. Symp.*, Vol. 3, 845–848, 2003.
10. Anob, P. V., K. P. Ray, and G. Kumar, "Wideband orthogonal square monopole antennas with semi-circular base," *Proc. IEEE Antennas Propag. Symp.*, Vol. 3, 294–297, 2001.
11. Wong, K. L., C. C. Huang, and W. S. Chen, "Printed ring slot antenna for circular polarisation," *IEEE Transactions on Antennas and Propagation*, Vol. 50, 75–77, 2002.
12. Ansari, J. A., A. Singh, and M. Aneesh, "Desktop shaped broadband microstrip patch antennas for wireless communications," *Progress In Electromagnetics Research Letters*, Vol. 50, 13–18, 2014.
13. Jan, J. Y. and J. W. Su, "Bandwidth enhancement of a printed wide-slot antenna with a rotated slot," *IEEE Transactions on Antennas and Propagation*, Vol. 53, 2111–2114, 2005.
14. Sze, J. Y. and K. L. Wong, "Bandwidth enhancement of a microstrip-line-fed printed wide-slot antenna," *IEEE Transactions on Antennas and Propagation*, Vol. 49, 1020–1024, 2001.
15. Jan, J. Y. and L. C. Wang, "Printed wideband rhombus slot antenna with a pair of parasitic strips for multiband applications," *IEEE Transactions on Antennas and Propagation*, Vol. 57, 1267–1270, 2009.